Portable Xray fluorescence spectroscopy as a tool for cyclostratigraphy

Journal Item

Geochemistry, Geophysics, Geosystems

AGU100 ADVANCING EARTH AND SPACE SCIENCE

TECHNICAL REPORTS: METHODS
10.1029/2018GC007582

Portable X-Ray Fluorescence Spectroscopy as a Tool for Cyclostratigraphy

Matthew Saker-Clark[1], David B. Kemp[2,3], and Angela L. Coe[1]

[1]School of Environment, Earth and Ecosystems Sciences, The Open University, Milton Keynes, UK, [2]School of Geosciences, University of Aberdeen, Old Aberdeen, UK, [3]Now at State Key Laboratory of Biogeology and Environmental Geology and School of Earth Sciences, China University of Geosciences, Wuhan, China

Key Points:
- Optimized portable X-ray fluorescence spectroscopy method allows fast and nondestructive production of elemental data from mudrock powders
- Analysis of portable X-ray fluorescence spectroscopy and combustion analysis data yield spectral peaks of similar statistical significance
- Portable X-ray fluorescence spectroscopy is suitable for producing cyclostratigraphic time series for identifying orbital forcing

Supporting Information:
- Supporting Information S1
- Table S1
- Table S2
- Table S3

Correspondence to:
D. B. Kemp,
davidkemp@cug.edu.cn

Citation:
Saker-Clark, M., Kemp, D. B., & Coe, A. L. (2019). Portable X-ray fluorescence spectroscopy as a tool for cyclostratigraphy. *Geochemistry, Geophysics, Geosystems*, *20*. https://doi.org/10.1029/2018GC007582

Received 29 MAR 2018
Accepted 3 APR 2019
Accepted article online 12 APR 2019

Abstract Cyclostratigraphic studies are used to create relative and high-resolution time scales for sedimentary successions based on identification of regular cycles in climate proxy data. This method typically requires the construction of long, high-resolution data sets. In this study, we have demonstrated the efficacy of portable X-ray fluorescence spectroscopy (pXRF) as a nondestructive method of generating compositional data for cyclostratigraphy. The rapidity (100 samples per day) and low cost of pXRF measurements provide advantages over relatively time-consuming and costly elemental and stable isotopic measurements that are commonly used for cyclostratigraphy. The nondestructive nature of pXRF also allows other geochemical analyses on the same samples. We present an optimized protocol for pXRF elemental concentration measurement in powdered rocks. The efficacy of this protocol for cyclostratigraphy is demonstrated through analysis of 360 Toarcian mudrock samples from North Yorkshire, UK, that were previously shown to exhibit astronomical forcing of [$CaCO_3$], [S], and $\delta^{13}C_{org}$. Our study is the first to statistically compare the cyclostratigraphic results of pXRF analysis with more established combustion analysis. There are strong linear correlations of pXRF [Ca] with dry combustion elemental analyzer [$CaCO_3$] ($r^2 = 0.7616$) and of pXRF [S] and [Fe] with dry combustion elemental analyzer [S] ($r^2 = 0.9632$ and $r^2 = 0.9274$, respectively). Spectral and cross-spectral analyses demonstrate that cyclicity previously recognized in [S], significant above the 99.99% confidence level, is present above the 99.92% and 99.99% confidence levels in pXRF [S] and [Fe] data, respectively. Cyclicity present in [$CaCO_3$] data above the 99.96% confidence level is also present in pXRF [Ca] above the 98.12% confidence level.

Plain Language Summary As the Earth rotates around the Sun, its orbit subtly changes over tens of thousands of years, and this controls Earth's climate. Earth's climate, in turn, influences the amount and type of sediment that gets deposited. These orbital changes can be recognized in sedimentary rocks as cyclic variations in chemistry. The cycles can be used to calculate how long it took to deposit sediments and are known as cyclostratigraphy. To recognize and measure cycles in the rock record typically requires hundreds of expensive and time-consuming analyses. In this study we improved a method of analyzing the chemistry of rocks using a portable X-ray fluorescence instrument. We used 360 samples of mudrock to statistically compare our new method using the portable X-ray instrument with the results determined previously by more time-consuming and more expensive combustion methods. Our study has shown for the first time that the cyclostratigraphy data produced using this portable X-ray tool are mathematically indistinguishable from these conventional chemical methods. This study is important because it shows that it is possible to more cheaply and efficiently construct robust cyclostratigraphic time scales using the X-ray instrument. Such cyclostratigraphic time scales can be used to understand the rate of Earth processes such as climate change and evolution of organisms.

1. Introduction

The construction of high-resolution geological time scales is important for understanding the duration, timing, and rapidity of Earth system processes such as paleoenvironmental change and evolution. Cyclostratigraphy is an effective method for producing high-resolution relative time scales in sedimentary successions. Cyclostratigraphic studies typically require construction of long, high-resolution, and regularly spaced climate proxy data in order to accurately resolve astronomical cycles (e.g., Weedon, 2003).

X-ray fluorescence spectroscopy (XRF) of sedimentary rocks, particularly using core scanners, has long been used as a chemostratigraphic and palaeoenvironmental tool (e.g., Algeo & Maynard, 2008; Kujau et al., 2010;

Kylander et al., 2011, 2012; Naeher et al., 2013; Weltje & Tjallingii, 2008; Wilhelms-Dick et al., 2012). Recent studies have commented on the use of portable XRF (pXRF) in sedimentary rock analyses, particularly for linking elemental changes to stratigraphic and paleoclimatic observations, and the calibration of pXRF instruments to other elemental analyzers (Dahl et al., 2013; de Winter et al., 2017; Ibañez-Insa et al., 2017; Kessler & Nagarajan, 2012; Lenniger et al., 2014; Mejia-Pina et al., 2016; Quye-Sawyer et al., 2015; Rowe et al., 2012; Thibault et al., 2018). The ability to measure elemental concentrations, and sensitivity of modern pXRF instruments, provides a clear rationale for employing pXRF analysis for cyclostratigraphy (e.g., Ruhl et al., 2016; Sinnesael et al., 2018; Thibault et al., 2018). The merits of using pXRF analysis for cyclostratigraphy have been discussed by Sinnesael et al. (2018). To date, however, the efficacy of pXRF as a cyclostratigraphic tool has not been quantitatively or statistically compared to established techniques.

Traditional techniques for constructing cyclostratigraphic time series focus on relatively time-consuming, destructive, and costly methods such as stable C and O isotopes, grain size, and elemental concentration analyses such as total organic carbon, S, and $CaCO_3$(e.g., Cleaveland et al., 2002; Holbourn et al., 2007; Liebrand et al., 2016; Vandenbergher et al., 1997; Zachos et al., 2010). Cheaper, quicker methods, such as magnetic susceptibility and color analyses, have also been used in cyclostratigraphy (e.g., Boulila et al., 2008; Boulila et al., 2014; Kemp & Coe, 2007). However, these data only indirectly reflect compositional variation that may be climate forced, potentially limiting their widespread effectiveness and interpretation in cyclostratigraphy.

Elemental analysis using pXRF tools has several potential advantages over more traditional data-gathering methods, owing primarily to the ability to produce large, high-precision data sets of elemental concentrations quickly and also relatively cheaply. Optimal analysis times are typically a few minutes per sample (de Winter et al., 2017; Quye-Sawyer et al., 2015). Additionally, portability of the instrument allows use in both the laboratory and field. Both powdered and solid samples can be analyzed, as well as exposure/core material. Because pXRF analysis is nondestructive, analyzed samples can also be used for other purposes, facilitating the generation of multiproxy data sets on exactly the same samples and thereby removing any possible errors associated with stratigraphic position or rock homogeneity.

In this study, we have quantitatively investigated the efficacy of pXRF for cyclostratigraphy for the first time by statistically comparing the results of cyclostratigraphic analysis from pXRF data to the cyclostratigraphic analysis of data gathered on exactly the same samples using more established combustion analysis. To do this, we have analyzed the 360 Toarcian (Early Jurassic) samples of powdered mudrock collected from North Yorkshire, UK, that were used in previous cyclostratigraphic studies (Kemp et al., 2005, 2011). We have directly compared the pXRF [Ca], [S], and [Fe] data and the previously gathered [$CaCO_3$] and [S] data from a dry combustion elemental analyzer from Kemp et al. (2005, 2011). Additionally, the results of spectral and cross-spectral analyses of these data sets, and subsequent statistical analyses of data quality, have been used to assess the efficacy of pXRF analyses for cyclostratigraphy. Second, we have conducted tests on the effects of varying sample thickness and sample receptacle size on the elemental analysis of rock standards. We used these results to refine the laboratory protocol for pXRF analysis of mudrock powders, which provide high sample homogeneity and a smooth sample surface, allowing production of highly precise and accurate data.

2. Materials and Methods

A Niton XL3t GOLDD+ pXRF analyzer was used in this study in Soils Mode, with standard internal calibration. In this mode, the instrument can quantify the concentration of a range of elements between the atomic masses of 24 and 238, dependent on the concentrations in the analyzed sample and conditions of analysis. Individual analysis times were 130 s based on manufacturer recommendations for optimizing precision with efficient analysis time. This analysis time is also consistent with that of Dahl et al. (2013), who conducted tests on this aspect of the method and demonstrated precise results from 120-s analyses. Following the manufacturer's integral settings, the first 60 s of analysis was carried out at 50 kV and 40 μA, followed by 60 s at 20 kV and 100 μA, and 10 s at 50 kV and 40 μA. The powdered samples were placed in an upturned vial, with the vial opening covered tightly in cling film and placed on the instrument aperture in a proprietary laboratory stand (see supporting information for photograph of the experimental setup). This method follows that outlined by Dahl et al. (2013).

Calibration of pXRF data was performed by comparing data from the Niton XL3t GOLDD+ pXRF to those from an ARL 8420+ dual goniometer wavelength-dispersive XRF and a Leco CNS-2000 dry combustion analyzer, from analyses of 29 Toarcian mudrock samples. Linear regression coefficients were determined by the least squares method (see supporting information). These coefficients were used to adjust pXRF data toward a 1:1 correlation with the ARL wavelength-dispersive XRF or Leco CNS-2000 data. These adjusted data are termed *calibrated pXRF data*.

In order to test the potential effects of the cling film membrane used in powder analysis, a pressed internal standard XRF powder pellet of Ailsa Craig microgranite from Scotland, UK (named AC-E; Potts et al., 1992; Godindaraju, 1987; see supporting information for elemental ranges), was repeatedly ($N = 10$) analyzed uncovered and with two types of cling film covering: polyvinyl chloride (PVC) containing and non-PVC (low-density polyethylene; section 3.1). This pellet was produced by combining 10 g of sample powder with 0.7-ml polyvinylpyrollidone/methylcellulose binder and pressing at 7–9 t/in.^{2} before drying at 110 °C.

Accurate matrix effect correction in XRF analysis, including Compton normalization, requires an element-specific minimum sample thickness, known as the Compton critical penetration depth (Potts & Webb, 1992). This matrix effect correction is carried out internally by the Niton pXRF instrument during analysis. To assess the effects of powder depth on pXRF-measured elemental concentrations, an internal powdered mudrock standard (DKJ1, see supporting information for elemental ranges) was analyzed repeatedly in upturned borosilicate glass vials, covered in non-PVC cling film, of both 7- and 20-ml volume, using 3-,5-,7-,9-,11-,13-,15-, and 20-mm powder thicknesses.

The optimized pXRF method (section 3.1) was applied to 360 samples of lower Toarcian (Lower Jurassic) mudrock. Aliquots of exactly the same samples were used in previous geochemical and cyclostratigraphic studies of the interval (Kemp et al., 2005, 2011). They were collected from Port Mulgrave and Hawsker Bottoms, near Whitby, North Yorkshire, UK (54°32′48.64″N, 00°45′59.50″W and 54°27′29.89″N, 00°33′25.62″W, respectively) every 2.5 cm between 1.30 m above and 7.81 m below the base of the *Harpoceras exaratum* ammonite subzone, as defined by Howarth (1992). Samples were collected from the outcrop using a cordless drill with an 8-mm masonry drill bit. Time series analysis of [$CaCO_3$], [TOC], [S], and $\delta^{13}C_{org}$ data from these samples has shown regular ~75-cm wavelength cycles attributable to astronomical forcing (Kemp et al., 2011). Long-term analytical precision during this pXRF study was quantified by repeat measurement ($N = 208$) of internal standard DKJ1.

To assess data accuracy using the pXRF method, we compared the [Ca] and [S] data from pXRF analyses of the 360 samples to the Leco CNS-2000 dry combustion elemental analyzer-derived [$CaCO_3$] and [S] data from Kemp et al. (2011), respectively. Because of the direct correlation between [Fe] and [S] for these samples due to pyrite being the dominant Fe-bearing phase (Kemp et al., 2011), pXRF [Fe] data were compared with Leco [S] data (Kemp et al., 2011). The same Leco dry combustion elemental analyzer was used to measure the 29 Toarcian mudrock samples, used for calibration of pXRF data. The power spectra results from the pXRF analyses of the 360 samples were compared to those from aliquots of the same samples from Kemp et al. (2011). Cross-spectral analysis of data from the two instruments was used to investigate differences in coherency and phase between the two methods. Power spectral estimation was carried out using the multitaper method (Thomson, 1982; Weedon, 2003), with four tapers used. Statistical significance of peaks in these spectra was assessed by least squares fitting of first-order autoregressive background noise models to the log power spectra, following methods outlined in Weedon (2003). Filtering was carried out using a Gaussian band-pass filter in Analyseries software (Paillard et al., 1996).

3. Results

3.1. Protocol Development

Measured values of the AC-E XRF powder pellet covered with non-PVC cling film membrane are within error ($\pm 2\sigma$) of those measured with no membrane, for all elements where analyses registered values above detection limits to allow precision (2σ) to be established (Table 1). Covering the AC-E powder pellet with PVC-containing cling film reduced measured values of [Fe], [Ca], [K], and [Ti], compared to analysis of the uncovered powder pellet. [Fe] is proportionally reduced by ~10%, from 1.192% to 1.073%; [Ca] is proportionally reduced by ~32%, from 0.240% to 0.163%; [K] is proportionally reduced by ~50%, from

Table 1
pXRF-Measured Elemental Concentrations and Precision for an XRF Powder Pellet Sample of the AC-E

Membrane	PVC-cling film		Non-PVC cling film		None	
Element	Mean concentration	Precision (2σ)	Mean concentration	Precision (2σ)	Mean concentration	Precision (2σ)
S (%)	0.384	0.037	<LOD	—	<LOD	—
Fe (%)	1.073	0.020	1.185	0.028	1.192	0.028
Ca (%)	0.163	0.008	0.228	0.020	0.240	0.021
Zr (%)	0.120	0.002	0.121	0.002	0.122	0.002
K (%)	1.988	0.057	3.863	0.096	3.999	0.097
Ti (ppm)	317.191	39.664	442.295	53.786	467.727	44.440
Cr (ppm)	73.749	32.150	111.776	23.712	97.051	18.958
Mn (ppm)	281.820	60.048	299.379	52.140	314.871	77.606
Zn (ppm)	194.436	20.648	189.954	15.063	198.952	16.028
Pb (ppm)	37.221	5.884	39.316	4.049	36.815	6.191
Th (ppm)	21.869	2.813	22.700	4.292	23.204	5.640
Rb (ppm)	128.958	5.762	129.484	4.602	130.822	5.033
Y (ppm)	214.522	10.217	216.549	8.182	217.745	4.721
Nb (ppm)	82.741	6.186	82.792	4.517	82.811	3.557
Mo (ppm)	6.200	2.222	6.105	1.531	6.963	1.854

Note. Sample was covered by non-PVC cling film, covered by PVC cling film, or not covered at all (none). Elements where too few results above instrument LODs were obtained to calculate precision (2σ) have been omitted. Mean concentration and 2σ precision data are calculated from results of 10 repeat measurements. pXRF = portable X-ray fluorescence spectroscopy; XRF = portable X-ray fluorescence spectroscopy; AC-E = Ailsa Craig microgranite; PVC = polyvinyl chloride; LOD = limit of detection.

3.999% to 1.988%; and [Ti] is proportionally reduced by ~32%, from 467.727 to 317.191 ppm (Table 1). Conversely, the use of PVC-containing cling film to cover the AC-E powder pellet increased [S] concentrations. [S] was below the limit of detection of the instrument when the pellet was measured with no membrane, and 0.384% when the pellet was covered with a PVC-containing membrane.

Using the internal mudrock standard DKJ1, we found that at powder depths of ≥9-mm pXRF data for [Mo], [Nb], [Zr], [Y], [Sr], [Fe], [Rb], and [As] are consistent and independent of vial size (Figure 1). Below this depth threshold, concentrations increase with decreasing powder thickness. Similarly, [Ag], [Cd], [Sn], [Sb], and [Cs] data are independent of vial size and consistent within error (±2σ) at powder depths ≥9 mm. However, these data show negative values and decreasing concentration with decreasing powder thickness below 9 mm (Figure 1). [Ba] also shows decreasing concentration with decreasing powder thickness below 9 mm, above which data are consistent and within error, but [Ba] is consistently ~500 ppm higher when analyzed in 7-ml vials compared to 20-ml vials (Figure 1). [Cu], [Hg], [Co], [U], [Mn], [Cr], [V], [Ti], [Sc], [W], [K], [S], [Zn], [Se], [Pb], and [Th] data remain mostly within error (±2σ) at all powder thicknesses and the two vial sizes, showing no systematic variation in relation to these parameters (Figure 1). At powder thicknesses of 7 mm and above, [Ca] and [Ni] are consistent, showing no variation with powder thickness or vial size (Figure 1). For powder thickness of <7 mm in 20-ml vials, [Ca] is elevated compared to that from equivalent samples analyzed in 7-ml vials, while the opposite trend is observed in [Ni].

The following optimized protocol for the pXRF analysis of mudrocks was developed based on the findings presented above:

1. Produce 2–5 g of very fine grained, homogenized powder from the sample.
2. Place the sample powder in a glass vial of sufficient diameter to cover the aperture of the instrument. Ensure that the depth of the powder is at least 10 mm. Tightly cover the vial opening in a single layer of non-PVC cling film.
3. Place the upturned vial directly on the aperture of the pXRF instrument held in a laboratory stand where possible (see supporting information).
4. Analyze the sample using the pXRF.
5. Apply postanalysis linear best fit calibration to the results using regression coefficients derived from a suite of reference materials of similar matrix to the study samples and whose composition encompasses the range of the study samples (in accordance with Rowe et al., 2012, and de Winter et al., 2017).

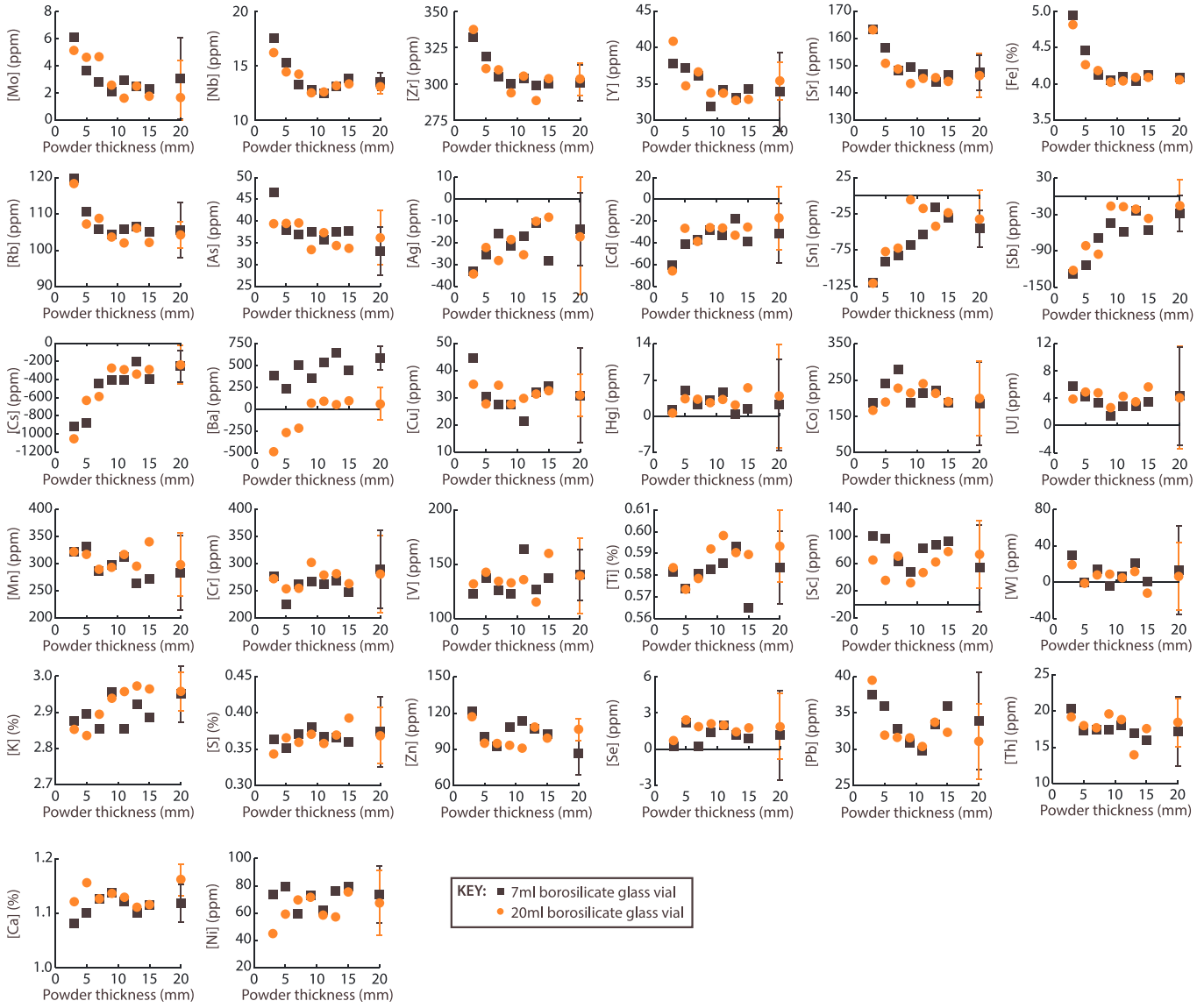

Figure 1. Graphs to show effect of changing analyzed powder thickness on measured (noncalibrated) elemental concentrations. Elemental concentrations for all measured elements of a powdered mudrock standard (DKJ1), measured in 20- and 7-ml glass vials at powder thicknesses of 3, 5, 7, 9, 11, 13, 15, and 20 mm. Error bars show $\pm 2\sigma$ uncertainty. Note that for many of the elements a thickness of >9 mm is required for consistent data.

3.2. Application of the Protocol to Cyclostratigraphy: Toarcian Case Study

3.2.1. Data Reproducibility and Calibration Errors

Long-term analytical precision of pXRF measurements of DKJ1 ($N = 208$) was 0.15%, 0.058%, and 0.041% for Fe, Ca, and S, respectively (2σ). For comparison, analytical precision (2σ) for dry combustion elemental analyzer measurements of DKJ1 for C and S abundance was better than 0.03 and 0.06 wt%, respectively (Kemp et al., 2011). Calibration error is quantified as the difference between expected and calibrated pXRF values for a given sample elemental concentration. Calibration errors were better than 0.302%, 0.340%, and 0.889% for Fe, Ca, and S measurements, respectively.

3.2.2. Comparison to Elemental Analyzer Data

There is strong positive linear correlation for [S] ($r^2 = 0.9632$) between calibrated data from pXRF and those produced using a Leco dry combustion elemental analyzer for the 360 early Toarcian mudrock samples (supporting information Figure S2). The data sets also show similar relative changes throughout the section. However, pXRF [S] is mostly greater than Leco elemental analyzer-measured [S], with a mean difference of 0.235% (Figure 2). Similarly, calibrated pXRF [Fe] data show a very strong linear correlation with [S] from

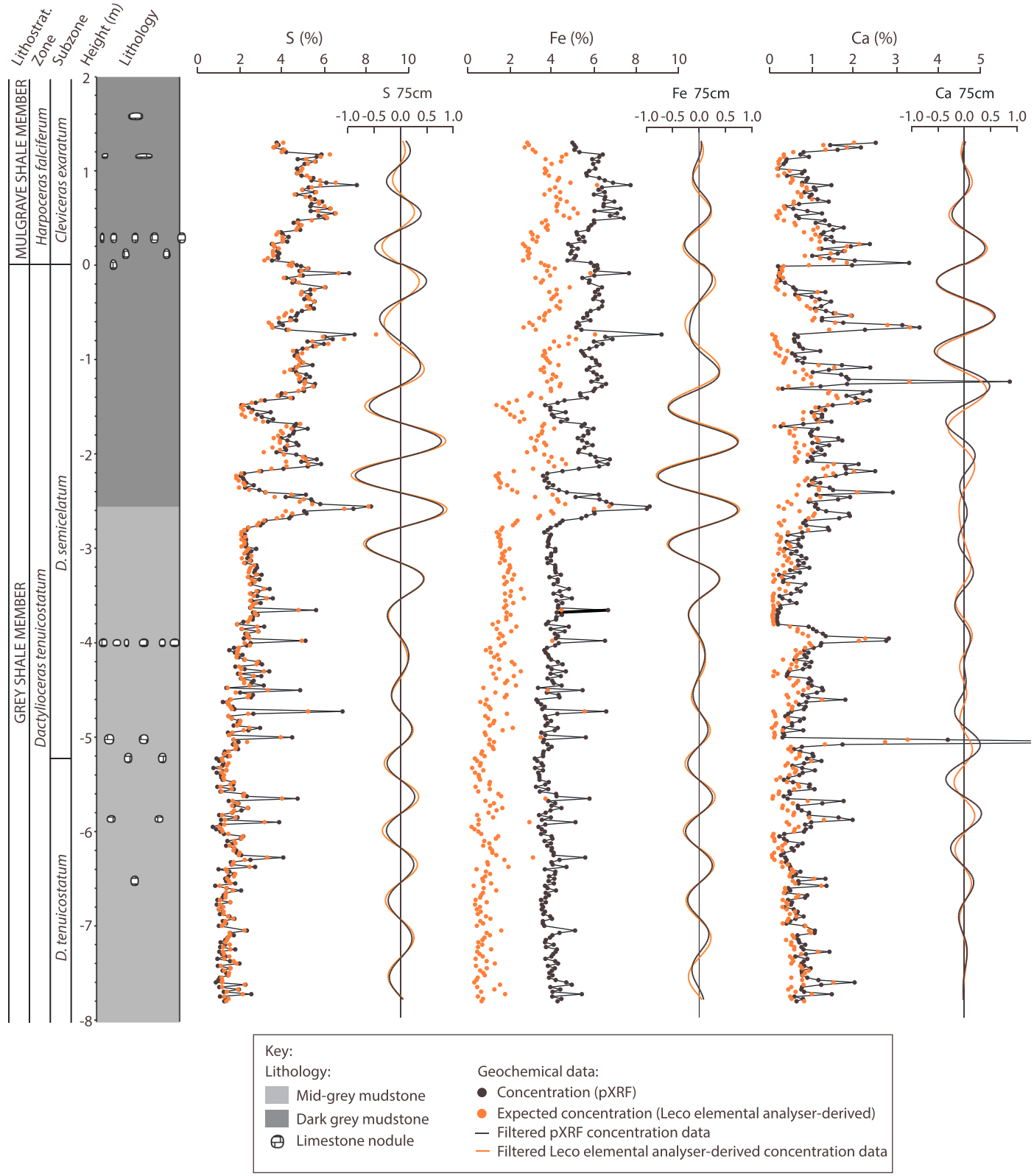

Figure 2. Comparison of [S], [Fe], and [Ca] data from portable X-ray fluorescence spectroscopy (pXRF) analyses with equivalent Leco elemental analyzer-derived data alongside biostratigraphy and lithostratigraphy from early Toarcian succession from near Whitby, Yorkshire, UK. Filtered elemental data are also shown. Filtering was performed using a Gaussian band-pass filter in Analyseries (center frequency = 0.0133, bandwidth = 0.0028). Leco elemental analyzer data and lithology are from Kemp et al. (2011). Lithostratigraphy and biostratigraphy are from Howarth (1992).

both Leco analyzer and pXRF measurements ($r^2 = 0.9274$ and 0.9237, respectively). [Fe] data derived from Leco elemental analyzer [S], assuming measured [S] is entirely from pyrite (see Kemp et al., 2011; Figure 2), show equivalent relative changes through the section to pXRF [Fe]. However, pXRF [Fe] is consistently greater than Leco elemental analyzer-derived [Fe], with a mean difference of 2.47% (Figure 2).

In order to compare calibrated pXRF [Ca] data with an independent measurement of [Ca], we assumed that $CaCO_3$ is the only inorganic carbon mineral phase. This is supported by the absence of siderite in the studied stratigraphic interval (Kemp et al., 2011), which would represent the only other plausible source of inorganic C that would not be detected by Leco dry combustion elemental analyzer analysis. pXRF [Ca] data and [Ca] derived from dry combustion elemental analyzer inorganic C measurements show a weaker linear correlation ($r^2 = 0.7616$) compared to [Fe] and [S]. These Ca data sets show similar relative changes through the section, but pXRF [Ca] is greater than dry combustion elemental analyzer-derived [Ca], with a mean difference of 0.359% (Figure 2).

3.2.3. Time Series Analysis

Power spectral analysis and significance testing indicate that a 75-cm wavelength cyclicity is present in pXRF [S] and [Fe] data (Figure 3) above the 99.92% and 99.99% confidence levels, respectively (Figure 3). A 75-cm cyclicity in dry combustion elemental analyzer [S] over the same interval was found to be significant above the 99.99% by Kemp et al. (2011). For further discussion of the possible origins of this cyclicity, see Kemp et al. (2005, 2011), Huang and Hesselbo (2014), and Boulila et al. (2014). Cross-spectral analysis demonstrates that the cyclicity observed in pXRF [S] and [Fe] is coherent and in phase with that observed in dry combustion elemental analyzer [S] data, with coherency above the 98.62% and 98.69% confidence levels, respectively (Figure 3). This demonstrates a consistent in-phase relationship (Figure 3), which is also readily apparent from similarities in filtered data (Figure 2).

Spectral analysis of pXRF-measured [Ca] data shows a 75-cm wavelength regular cyclicity across the interval from −7.81 to 1.30 m (Figure 3). A 75-cm-wavelength regular cyclicity in Leco dry combustion elemental analyzer-derived [$CaCO_3$] was demonstrated by Kemp et al. (2011) over the same interval. The pXRF [Ca] spectral peak associated with this cyclicity is significant at the 98.12% confidence level, compared to 99.96% for the Leco elemental analyzer [$CaCO_3$] power spectrum (Figure 3). Cross-spectral analysis shows these cyclicities are coherent above the 98.34% significance level and are in phase (Figure 3b). This in-phase relationship can also be seen through comparison of filtered data (Figure 2). Frequencies in the power spectra for pXRF [Ca] and Leco elemental analyzer [$CaCO_3$] are mostly coherent above the 95% confidence level and are in phase at frequencies below 12 cycles/m (Figure 3). At frequencies above 12 cycles/m, where no statistically significant cycles are observed, coherency drops and fluctuates greatly (Figure 3. Correspondingly, there is no consistent or reliable phase relationship, because phase error is dependent on coherency (Weedon, 2003).

4. Discussion

4.1. Refined Protocol for pXRF Analysis of Mudrocks

The use of finely powdered samples in our optimized protocol ensures high sample homogeneity in terms of composition and grain size, while also obviating heterogeneities in physical properties such as cementation. The use of a powder also ensures a smooth sample surface, which reduces errors caused by the nondetection of fluorescence X-rays that do not reach the sensor due to space between sample and instrument (Andersen et al., 2013). Because pXRF analysis is nondestructive, the powders can be used for other analyses to produce multiproxy data sets from precisely the same samples.

Our results show that the membrane used to contain the powdered samples and prevent contamination needs to be of appropriate composition to prevent undesirable effects on the measurements. We found that chlorine-containing (PVC) cling films affect the quality of pXRF data, reducing [Fe], [Ca], [K], and [Ti] and increasing [S]. Non-PVC cling film has no significant effect on elements measured in this study. The consistency of results between analyses made with non-PVC cling film and those without a membrane covering suggests that non-PVC cling film is largely transmissive to X-rays.

Analyses of a powdered mudrock internal standard (DKJ1) using pXRF show that powder thicknesses of >9 mm are required to produce consistent, reproducible elemental data (Figure 1). This finding is in

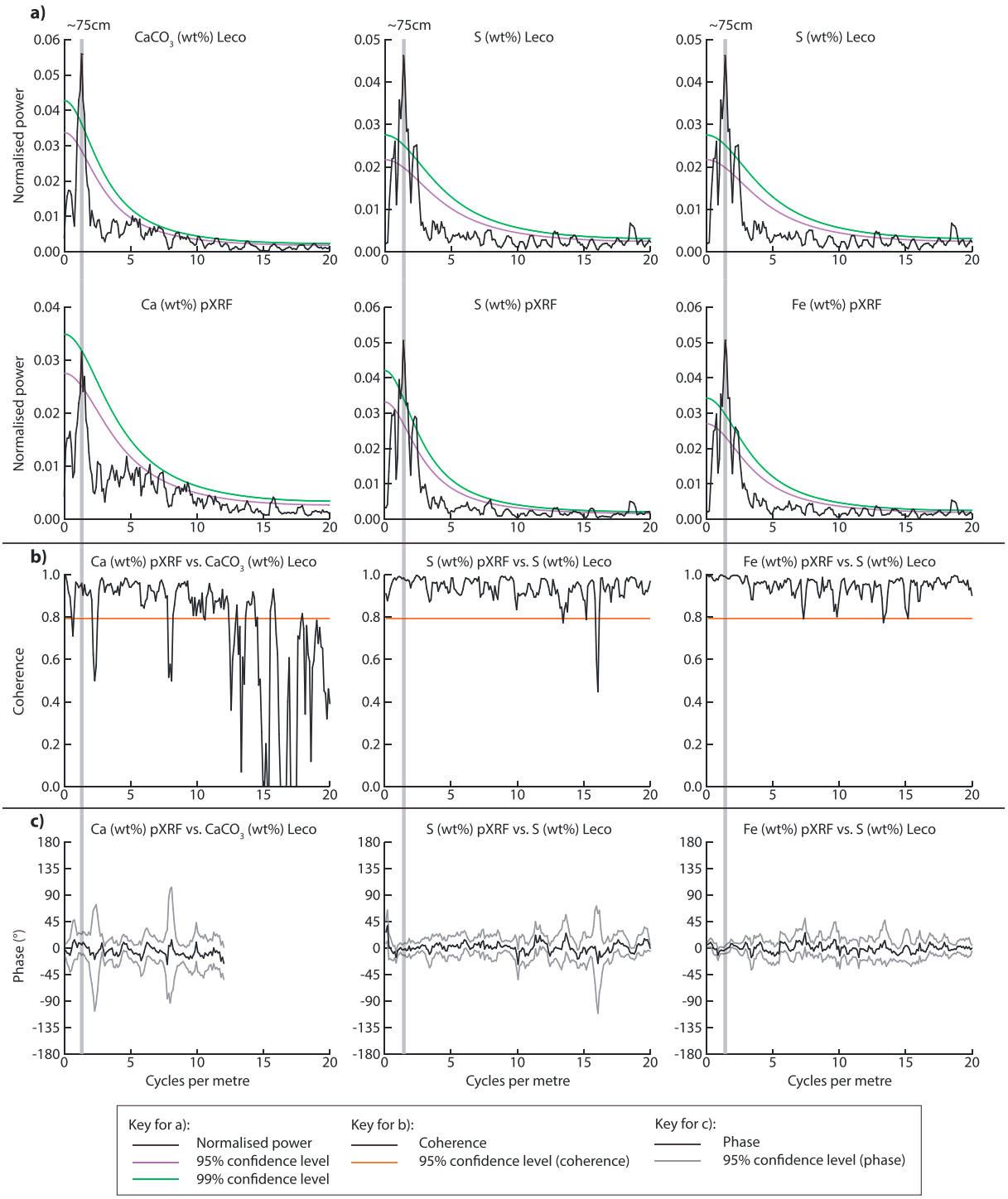

Figure 3. (a) Power spectra of Leco elemental analyzer-derived [$CaCO_3$] and [S] and power spectra of pXRF [Ca], [S], and [Fe]. Bandwidth = 0.437 cycles/m. (b) Coherence and (c) phase relationships of pXRF [Ca] versus Leco [$CaCO_3$], pXRF [S] versus Leco [S], and pXRF [Fe] versus Leco [S]. Prior to power spectral analysis, all data were detrended through removal of a linear fit. pXRF = portable X-ray fluorescence spectroscopy.

contrast to the minimum thickness recommendations by Dahl et al. (2013; >4 mm), Mejia-Pina et al. (2016; >4 mm), and de Winter et al. (2017; >7 mm). Incorrect Compton normalization (i.e., normalization to the intensity of the Compton scatter peak to correct for matrix effects) is likely to be the cause of the observed increase in [Fe], [As], [Rb], [Sr], [Y], [Zr], [Nb], and [Mo] and decrease in [Ag], [Cd], [Sn], [Sb], [Cs], and

[Ba] with increasing powder depth in the analysis of samples with <9 mm of powder (Dahl et al., 2013; Potts & Webb, 1992). Such error is not observed in [S], [K], [Ti], [Mn], [Pb], [U], [Th], [Se], [Hg], [W], [Cu], [Co], [Sc], [V], [Cr], [Ca], and [Ni] data. It is likely that for [S], [K], [Ca], [Sc], [Ti], [V], [Cr], and [Mn], the thicknesses investigated here exceed the Compton critical penetration depths for these elements, as Compton normalization error is only observed in heavier elements and Compton critical penetration depth increases with increasing atomic weight (Potts & Webb, 1992). In contrast, for [Pb], [U], [Th], [Se], [Hg], [W], [Cu], [Co], and [Ni], Compton normalization error is not observed, as any error of this kind is within the large analytical error. This error is likely related to the instrument limitations, such as measured quantities being close to element-specific detection limits of the pXRF instrument, which prevent the use of this setup for reliable measurement of low concentrations of these elements. Observed negative [Ba], [Cs], [Sb], [Sn], [Cd], and [Ag] data, which become increasingly negative with decreasing powder thickness below 9 mm, are likely related to inappropriate calibration combined with Compton normalization error. At powder thicknesses >9 mm, there is no variation in [Ba], [Cs], [Sb], [Sn], [Cd], and [Ag] data. This suggests that these elements can be reliably measured using powder depths of >9 mm with appropriate calibration. Measurements of all elements apart from Ba are not affected by the volume of analyzed sample (7- versus 20-ml vial). Therefore, in the case of the Niton pXRF, very small samples (~0.75 g) can be used in 7-ml vials to ensure the critical powder thickness of >9 mm. Further work is required to understand why Ba concentration is affected by the volume of the analyzed sample.

4.2. Quality of pXRF Data and Its Suitability for Use in Cyclostratigraphy

Based on analysis of 360 Toarcian mudrocks, a ~75-cm regular cyclicity of similar significance was revealed in spectral analysis of data collected by both pXRF ([S], [Fe], and [Ca]) and dry combustion elemental analyzer analyses ([S] and [$CaCO_3$]; Kemp et al., 2011). This observation is further supported by coherency similarities. Specifically, coherency is significant above the 98% confidence level, and there is an in-phase relationship between comparable/equivalent dry combustion elemental analyzer-derived and pXRF data at the 75-cm wavelength. Taken together, these results demonstrate that the pXRF data are suitable for cyclostratigraphy.

We have shown that pXRF analysis can be a statistically comparable suitable alternative to more expensive dry combustion or coulometric elemental analysis. However, our results do show small absolute differences between equivalent/comparable data sets. Differences between Leco dry combustion elemental analyzer- and pXRF-obtained [S] data (mean difference = 0.235%), and errors related to pXRF and Leco precision limits (0.041% and 0.06 wt%, respectively), are small in comparison to the absolute concentrations measured (1.09–8.48 wt%). The analysis of lower absolute concentrations may be affected more severely by accuracy and precision limitations of pXRF analysis and as the limits of detection of the pXRF instrument are approached.

The very strong positive linear correlation of pXRF [Fe] with both pXRF [S] and elemental analyzer [S] ($r^2 = 0.9237$ and 0.9274, respectively) emphasizes that pyrite is the dominant phase of Fe and S in the studied succession, as suggested by Kemp et al. (2011). However, the mean difference of 2.47% between pXRF [Fe] data and [Fe] derived from elemental analyzer [S] data cannot be attributed to total uncertainty in pXRF [Fe] (i.e., combined instrument precision limitations and calibration error), which is 0.452%. Instead, it is likely that pXRF analysis is also measuring some nonpyritic Fe, most likely from detrital mineral phases (e.g., ilmenite) or possibly due to small amounts of contamination from the sample extraction method that used a masonry (steel) drill bit.

The strong linear correlation between [Ca] measured using pXRF with predicted [Ca] derived from dry combustion elemental analyzer inorganic C data demonstrates that pXRF analyses are a high-accuracy alternative to $CaCO_3$ quantification using coulometer or dry combustion elemental analyzer C analysis. However, there is a mean difference between pXRF- and dry combustion elemental analyzer-derived Ca data of 0.359%. The calibration and precision limitations of the pXRF instrumentation are unlikely to be the cause of this discrepancy, as calculated uncertainty related to calibration error and instrument precision is generally smaller than the discrepancy observed (see section 3.2.1). Additionally, calibration against accepted values from the ARL wavelength-dispersive XRF machine means that our data should not be subject to [Ca] increases intrinsic to the use of energy-dispersive XRF pXRF instrumentation (Rowe et al., 2012). Rather, like in the Fe data, it is likely that the discrepancy is due to additional sources of Ca in the samples that are measured by pXRF analyses but are not included in estimates from $CaCO_3$ measurements based on

inorganic C analysis. These small data discrepancies may contribute to the reduced variability and slightly reduced statistical significance of cycles observed in this study.

Previously published analytical precision data for the Niton XL3t instrument (Brand & Brand, 2014) compare well with our own results. Equally, the reproducibility achievable by the Niton instrument is comparable to other available instruments (e.g., Brand & Brand, 2014). Thus, our protocol and the generation of high-quality cyclostratigraphic data should be applicable to other makes and models of modern handheld XRF instruments.

5. Conclusions

1. pXRF is suitable for constructing robust, long cyclostratigraphic time series and identifying orbital forcing. The method provides a cheap, fast, and nondestructive alternative to elemental analysis techniques commonly used in cyclostratigraphic studies.
2. Cycles of 75 cm seen in [$CaCO_3$] and [S] Leco data with significance levels above 99.96% and 99.99%, respectively, are observed at similarly high significance levels in pXRF [Ca], [S], and [Fe] data (significance above the 98.12%, 99.92%, and 99.99% levels, respectively) from aliquots of the same samples.
3. The use of pXRF, using non-PVC cling film covering 10-mm thickness of rock powder in borosilicate glass vials, enables the collection of high-quality elemental concentration ([Ag], [As], [Ba], [Ca], [Cd], [Cr], [Cs], [Fe], [K], [Mn], [Mo], [Nb], [Rb], [S], [Sb], [Sc], [Sn], [Sr], [Ti], [V], [Y], and [Zr]) data for mudrocks.

Acknowledgments
Data referred to in this text can be found in Tables S1 to S4 in the supporting information to this manuscript. We thank Peter Webb for constructive discussions regarding the principles of X-Ray fluorescence spectroscopy. M. S.-C. was supported by a Natural Environmental Research Council (NERC) studentship grant NE/L002493/1. D. B. K. was funded by NERC Research Fellowship (grant NE/I02089X/1). We thank Nicolas Thibault and an anonymous reviewer for their helpful comments on an earlier version of this manuscript.

References

Algeo, T. J., & Maynard, J. B. (2008). Trace-metal covariation as a guide to water-mass conditions in ancient anoxic marine environments. *Geosphere*, *4*(5), 872. https://doi.org/10.1130/GES00174.1

Andersen, L. K., Morgan, T. J., Boulamanti, A. K., Lvarez, P., Vassilev, S. V., & Baxter, D. (2013). Quantitative X-ray fluorescence analysis of biomass: Objective evaluation of a typical commercial multi-element method on a WD-XRF spectrometer. *Energy and Fuels*, *27*(12), 7439–7454. https://doi.org/10.1021/ef4015394

Boulila, S., Galbrun, B., Huret, E., Hinnov, L. A., Rouget, I., Gardin, S., & Bartolini, A. (2014). Astronomical calibration of the Toarcian stage: Implications for sequence stratigraphy and duration of the early Toarcian OAE. *Earth and Planetary Science Letters*, *386*, 98–111. https://doi.org/10.1016/j.epsl.2013.10.047

Boulila, S., Hinnov, L. A., Huret, E., Collin, P. Y., Galbrun, B., Fortwengler, D., et al. (2008). Astronomical calibration of the Early Oxfordian (Vocontian and Paris basins, France): Consequences of revising the Late Jurassic time scale. *Earth and Planetary Science Letters*, *276*(1–2), 40–51. https://doi.org/10.1016/j.epsl.2008.09.006

Brand, N. W., & Brand, C. J. (2014). Performance comparison of portable XRF instruments. *Geochemistry: Exploration, Environment, Analysis*, *14*(2), 125–138. https://doi.org/10.1144/geochem2012-172

Cleaveland, L. C., Jensen, J., Goese, S., Bice, D. M., & Montanari, A. (2002). Cyclostratigraphic analysis of pelagic carbonates at Monte dei Corvi (Ancona, Italy) and astronomical correlation of the Serravallian-Tortonian boundary. *Geology*, *30*(10), 931. https://doi.org/10.1130/00917613(2002)030<0931:CAOPCA>2.0.CO;2

Dahl, T. W., Ruhl, M., Hammarlund, E. U., Canfield, D. E., Rosing, M. T., & Bjerrum, C. J. (2013). Tracing euxinia by molybdenum concentrations in sediments using handheld X-ray fluorescence spectroscopy (HHXRF). *Chemical Geology*, *360–361*, 241–251. https://doi.org/10.1016/j.chemgeo.2013.10.022

de Winter, N. J., Sinnesael, M., Makarona, C., Vansteenberge, S., & Claeys, P. (2017). Trace element analyses of carbonates using portable and micro-X-ray fluorescence: Performance and optimization of measurement parameters and strategies. *Journal of Analytical Atomic Spectrometry*, *32*, 1211–1223. https://doi.org/10.1039/C6JA00361C

Godindaraju, K. (1987). 1987 compilation report on the Ailsa Craig granite AC-E with the participation of the 128 GIT-IWG laboratories. *Geostandards Newsletter*, *12*, 119–201.

Holbourn, A., Kuhnt, W., Schulz, M., Flores, J.-A., & Andersen, N. (2007). Orbitally-paced climate evolution during the middle Miocene "Monterey" carbon-isotope excursion. *Earth and Planetary Science Letters*, *261*(3), 534–550. https://doi.org/10.1016/j.epsl.2007.07.026

Howarth, M. (1992). The ammonite family Hildoceratidae in the Lower Jurassic of Britain. *Monograph of the Palae-ontographical Society*, *145*, 1–106.

Huang, C., & Hesselbo, S. P. (2014). Pacing of the Toarcian oceanic anoxic event (Early Jurassic) from astronomical correlation of marine sections. *Gondwana Research*, *25*(4), 1348–1356. https://doi.org/10.1016/j.gr.2013.06.023

Ibañez-Insa, J., Perez-Cano, J., Fondevilla, V., Oms, O., Rejas, M., Fernandez-Turiel, J. L., et al. (2017). Portable X-ray fluorescence identification of the Cretaceous/Paleogene boundary: Application to the Agost and Caravaca sections, SE Spain. *Cretaceous Research*, *78*, 139–148. https://doi.org/10.1016/j.cretres.2017.06.004

Kemp, D. B., & Coe, A. L. (2007). A nonmarine record of eccentricity forcing through the Upper Triassic of southwest England and its correlation with the Newark Basin astronomically calibrated geomagnetic polarity time scale from North America. *Geology*, *35*(11). https://doi.org/10.1130/G24155A.1

Kemp, D. B., Coe, A. L., Cohen, A. S., & Schwark, L. (2005). Astronomical pacing of methane release in the Early Jurassic period. *Nature*, *437*(7057), 396–399. https://doi.org/10.1038/nature04037

Kemp, D. B., Coe, A. L., Cohen, A. S., & Weedon, G. P. (2011). Astronomical forcing and chronology of the early Toarcian (Early Jurassic) oceanic anoxic event in Yorkshire, UK. *Paleoceanography*, *26*, PA4210. https://doi.org/10.1029/2011PA002122

Kessler, F. L., & Nagarajan, R. (2012). A semi-quantitative assessment of clay content in sedimentary rocks using portable X-ray fluorescence spectrometry. *International Journal of Earth Sciences and Engineering*, *5*(2), 363–364.

Kujau, A., Nürnberg, D., Zielhofer, C., Bahr, A., & Röhl, U. (2010). Mississippi River discharge over the last ~560,000years—Indications from X-ray fluorescence core-scanning. *Palaeogeography, Palaeoclimatology, Palaeoecology*, *298*(3–4), 311–318. https://doi.org/10.1016/j.palaeo.2010.10.005

Kylander, M. E., Ampel, L., Wohlfarth, B., & Veres, D. (2011). High-resolution X-ray fluorescence core scanning analysis of Les Echets (France) sedimentary sequence: New insights from chemical proxies. *Journal of Quaternary Science*, *26*(1), 109–117. https://doi.org/10.1002/jqs.1438

Kylander, M. E., Lind, E. M., Wastegard, S., & Lowemark, L. (2012). Recommendations for using XRF core scanning as a tool in tephrochronology. *The Holocene*, *22*(3), 371–375. https://doi.org/10.1177/0959683611423688

Lenniger, M., Nøhr-Hansen, H., Hills, L. V., & Bjerrum, C. J. (2014). Arctic black shale formation during Cretaceous oceanic anoxic event 2. *Geology*, *42*, 799–802. https://doi.org/10.1130/G35732.1

Liebrand, D., Beddow, H. M., Lourens, L. J., Pälike, H., Raffi, I., Bohaty, S. M., et al. (2016). Cyclostratigraphy and eccentricity tuning of the early Oligocene through early Miocene (30.1–17.1 Ma): Cibicides mundulus stable oxygen and carbon isotope records from Walvis Ridge site 1264. *Earth and Planetary Science Letters*, *450*, 392–405. https://doi.org/10.1016/j.epsl.2016.06.007

Mejia-Pina, K. G., Huerta-Diaz, M. A., & González-Yajimovich, O. (2016). Calibration of handheld X-ray fluorescence (XRF) equipment for optimum determination of elemental concentrations in sediment samples. *Talanta*, *161*, 359–367. https://doi.org/10.1016/j.talanta.2016.08.066

Naeher, S., Gilli, A., North, R. P., Hamann, Y., & Schubert, C. J. (2013). Tracing bottom water oxygenation with sedimentary Mn/Fe ratios in Lake Zurich, Switzerland. *Chemical Geology*, *352*, 125–133. https://doi.org/10.1016/j.chemgeo.2013.06.006

Paillard, D., Labeyrie, L., & Yiou, P. (1996). Macintosh program performs time-series analysis. *Eos, Transactions American Geophysical Union*, *77*(39), 379. https://doi.org/10.1029/96EO00259

Potts, P. J., Tindle, A. G., & Webb, P. C. (1992). *Geochemical reference material compositions: Rocks, minerals, sediments, soils, carbonates, refractories and ores used in research and industry*. Caithness, Scotland and Boca Raton, FL:Whittles Publishing and Taylor & Francis. Retrieved from https://www.whittlespublishing.com/contact-us.asp, https://www.crcpress.com/

Potts, P. J., & Webb, P. C. (1992). X-ray fluorescence spectrometry. *Journal of Geochemical Exploration*, *44*(1-3), 251–296. https://doi.org/10.1016/0375-6742(92)90052-A

Quye-Sawyer, J., Vandeginste, V., & Johnston, K. J. (2015). Application of hand-heldenergy-dispersiveX-ray fluorescence spectrometry to carbonate studies: Opportunities and challenges. *Journal of Analytical Atomic Spectrometry*, *30*, 1490–1499. https://doi.org/10.1039/C5JA00114E

Rowe, H., Hughes, N., & Robinson, K. (2012). The quantification and application of handheld energy-dispersivex-ray fluorescence (ED-XRF) in mudrock chemostratigraphy and geochemistry. *Chemical Geology*, *324–325*, 122–131. https://doi.org/10.1016/j.chemgeo.2011.12.023

Ruhl, M., Hesselbo, S. P., Hinnov, L., Jenkyns, H. C., Xu, W., Riding, J. B., et al. (2016). Astronomical constraints on the duration of the Early Jurassic Pliensbachian Stage and global climatic fluctuations. *Earth and Planetary Science Letters*, *455*, 149–165. https://doi.org/10.1016/j.epsl.2016.08.038

Sinnesael, M., de Winter, N. J., Snoeck, C., Montanari, A., & Claeys, P. (2018). An integrated pelagic carbonate multi-proxy study using portable X-ray fluorescence (pXRF): Maastrichtian strata from the Bottaccione Gorge, Gubbio, Italy. *Cretaceous Research*, *91*, 20–32. https://doi.org/10.1016/j.cretres.2018.04.010

Thibault, N., Ruhl, M., Ullmann, C. V., Korte, C., Kemp, D. B., Gröcke, D. R., & Hesselbo, S. P. (2018). The wider context of the Lower Jurassic Toarcian oceanic anoxic event in Yorkshire coastal outcrops, UK. *Proceedings of the Geologists' Association*, *129*, 372–391. https://doi.org/10.1016/j.pgeola.2017.10.007

Thomson, D. J. (1982). Spectrum estimation and harmonic analysis. *Proceedings of the IEEE*, *70*(9), 1055–1096. https://doi.org/10.1109/PROC.1982.12433

Vandenbergher, N., Laenen, B., Van Echelpoel, E., & Lagrou, D. (1997). Cyclostratigraphy and climatic eustasy. Example of the Rupelian stratotype. *Comptes Rendus de l'Académie des Sciences-SeriesIIA-Earth and Planetary Science*, *325*(5), 305–315.

Weedon, G. P. (2003). *Time-series analysis and cyclostratigraphy: Examining stratigraphic records of environmental cycles*. Cambridge: Cambridge University Press.

Weltje, G., & Tjallingii, R. (2008). Calibration of XRF core scanners for quantitative geochemical logging of sediment cores: Theory and application. *Earth and Planetary Science Letters*, *274*, 423–438. https://doi.org/10.1016/j.epsl.2008.07.054

Wilhelms-Dick, D., Westerhold, T., Röhl, U., Wilhelms, F., Vogt, C., Hanebuth, T. J. J., et al. (2012). A comparison of mm scale resolution techniques for element analysis in sediment cores. *Journal of Analytical Atomic Spectrometry*, *27*(9), 1574. https://doi.org/10.1039/c2ja30148b

Zachos, J. C., McCarren, H., Murphy, B., Röhl, U., & Westerhold, T. (2010). Tempo and scale of late Paleocene and early Eocene carbon isotope cycles: Implications for the origin of hyperthermals. *Earth and Planetary Science Letters*, *299*, 242–249. https://doi.org/10.1016/j.epsl.2010.09.004